Lattice dynamical probe of charge order and antipolar bilayer stacking in $LuFe_2O_4$

X. S. Xu,[1,*] J. de Groot,[2] Q.-C. Sun,[1] B. C. Sales,[3] D. Mandrus,[3,4] M. Angst,[2] A. P. Litvinchuk,[5] and J. L. Musfeldt[1]
[1]*Department of Chemistry, University of Tennessee, Knoxville, Tennessee 37996, USA*
[2]*Institut für Festkörperforschung, JCNS and JARA-FIT, Forschungszentrum Jülich GmbH, D-52425 Jülich, Germany*
[3]*Materials Science and Technology Division, Oak Ridge National Laboratory, Oak Ridge, Tennessee 37831, USA*
[4]*Department of Materials Science and Engineering, University of Tennessee, Knoxville, Tennessee 37996, USA*
[5]*Texas Center for Superconductivity and Department of Physics, University of Houston, Houston, Texas 77204, USA*
(Received 13 May 2010; published 27 July 2010)

We investigated the infrared response of $LuFe_2O_4$ through the series of charge, magnetic, and structural transitions. All vibrational modes couple strongly to the charge order, whereas the LuO zone-folding modes are also sensitive to magnetic order and structural distortion. The dramatic splitting of the LuO_2 layer mode is attributed to charge-rich/poor proximity effects and its temperature dependence reveals the antipolar nature of the W layer pattern.

DOI: 10.1103/PhysRevB.82.014304 PACS number(s): 71.30.+h, 75.30.Kz, 78.20.Ci, 76.80.+y

I. INTRODUCTION

Multiferroics are materials that carry more than one ferroic order (e.g., magnetic and electric order), a relatively rare coincidence of functionalities that gives rise to rich physics, interesting tunability, and promising applications. $LuFe_2O_4$ is often cited as the prototypical electronically driven multiferroic.[1] Notable aspects include high ordering temperatures, large order parameters, orbitally induced magnetic anisotropy, and facile dielectric tunability in magnetic and electric fields.[2–6] On the other hand, many critical properties are controversial, for instance, ferroelectric vs antipolar bilayer ordering and the role of the lattice through the cascade of temperature-driven transitions.[3,7–10]

$LuFe_2O_4$ crystallizes in a rhombohedral ($R\bar{3}m$) structure with alternating Fe-containing double layers (often called Fe_2O_2 or W layers) and LuO_2 layers, each with triangular connectivity. Above 500 K, the Fe site charge is 2.5+, characteristic of a disordered phase with ferroelectric fluctuations. Two-dimensional Fe^{2+}/Fe^{3+} charge ordering (CO) appears below 500 K, three-dimensional (3D) charge order sets in at 320 K (T_{CO}) although fluctuations persist to much lower temperature, long-range magnetic order occurs below 240 K (T_N), and a magnetostructural transition is observed at 175 K (T_{LT}).[3,7,8,11–14] Local polarization emanates from the charge-order-induced charge imbalance in the W layer.[3] Order-by-fluctuation and electron-phonon coupling models have both been put forward as mechanisms for the development of the charge-ordered superstructure.[15,16] Since both charge order and magnetism originate from Fe site ordering, magnetoelectric coupling is strong.

To elucidate charge and bonding in a model charge ordered multiferroic, we investigated the lattice dynamics of $LuFe_2O_4$. What differentiates $LuFe_2O_4$ from other coupled materials such as α'-NaV_2O_5, $CuFeO_4$, TmSe, and many manganites and organic molecular solids is the combined presence of fluctuation, charge order/disorder, and frustration.[17,18] Our chosen technique, infrared vibrational spectroscopy, is a sensitive, microscopic probe of charge, structure, and bonding, and its fast time scale ($\sim 10^{12}$–10^{13} Hz) is well suited for the study of a fluctuating disordered system over a wide temperature range. We find that the lattice is very sensitive to charge order and magnetism in $LuFe_2O_4$. This interaction is best exemplified by LuO_2 mode splitting below T_{CO} which confirms antipolar bilayer stacking[19] (and rules out the previously supposed ferroelectric alignment). Moreover, charge order couples strongly to and competes with magnetism between T_N and T_{LT}, as illustrated by the behavior of the LuO_2 zone-folding modes. Finally, our measurements reveal an additional regime below 50 K that may be related to glassy state formation.

II. METHODS

Large $LuFe_2O_4$ single crystals were grown by floating-zone techniques.[7,8] Near-normal reflectance[20] was measured on the $(001)_h$ plane employing a Bruker 113v Fourier transform infrared spectrometer, covering the frequency range from 30–5000 cm^{-1}(3.7–0.62 eV) at 41 different temperatures between 10 and 500 K. Room-temperature reflectance was also collected up to 6 eV using a Perkin Elmer λ-900 grating spectrometer. The imaginary part of the dielectric function, $\varepsilon_2(\omega)$, was calculated from the measured reflectance by a Kramers-Kronig analysis.[21,22] Complementary transmittance experiments (77–300 K) on powder samples embedded in a paraffin matrix allowed us to calculate absorption, $\alpha(\omega)$, directly.[21] Standard peak-fitting techniques were employed as appropriate.[23] Lattice dynamical calculations were performed within the shell model approximation using the GULP package which includes long-range Coulomb interactions along with short-range ionic potentials.[24] The model is proven to adequately describe the lattice dynamics of ionic materials, metal oxides, in particular.[25,26] Ionic valence was varied to provide a reasonable match with the experimental spectra.

III. RESULTS AND DISCUSSION

A. Structure and symmetry

The rhombohedral ($R\bar{3}m$) high-temperature structure of $LuFe_2O_4$ is usually described in a hexagonal setting with the

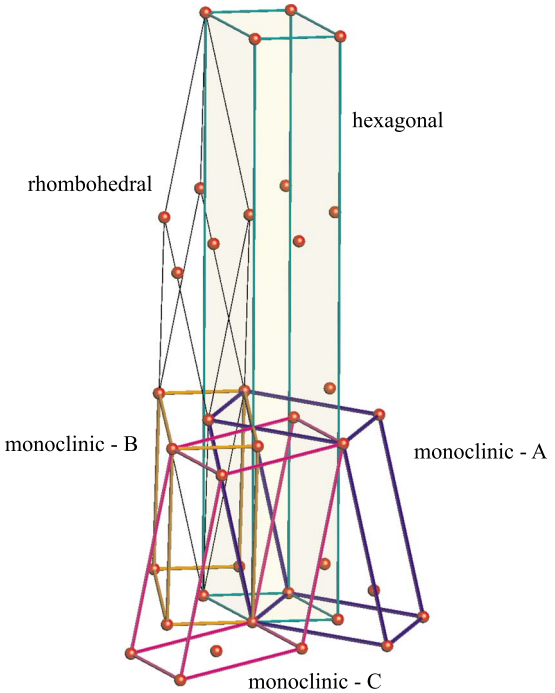

FIG. 1. (Color online) Different cells describing the high temperature $LuFe_2O_4$. Apart from the primitive rhombohedral and the *R*-centered hexagonal (standard setting) cells the lattice can also be described by one of three *C*-centered monoclinic cells, which are rotated by 120° with respect to each other. Cells describing the charge order in the three domains are obtained from the latter by tripling the monoclinic *b* and doubling the monoclinic *c* axes (omitted for clarity).

R-centered cell containing three Fe/O double layers. Alternative cells describing the same structure are possible, including *C*-centered monoclinic cells containing only one Fe/O double layer (see Fig. 1). Charge ordering breaks the threefold rotational symmetry, lowering the symmetry to monoclinic as mentioned in Ref. 8. One consequence of the loss of threefold rotation symmetry is the occurrence of three symmetry-equivalent structures, described with cells rotated by 120° relative to each other. Each of the latter corresponds to a CO domain associated with one of the symmetry-equivalent propagation vectors and the occurrence of multiple CO domains implies a correspondingly twinned sample.

For each domain, the CO superstructure can be described by a multiple of one of the three *C*-centered monoclinic cells shown in Fig. 1. The CO propagation vector of, e.g., $(\frac{1}{3}\frac{1}{3}\frac{3}{2})_h$ becomes in the appropriate monoclinic cell $(0\frac{1}{3}\frac{1}{2})_m$, i.e., the CO triples the monoclinic cell along *b* and doubles it along *c*.[27] This sixfold enlarged CO cell is again *C* centered and the CO has space group $C2/m$. Bragg reflections collected by single-crystal x-ray diffraction are indeed well described by three twins of *C*-centered cells ($a=5.95$ Å, $b=10.32$ Å, $c=17.31$ Å, $\beta=103.2°$) with $C2/m$ symmetry.[28] The structural twinning places strong restrictions on the lattice parameters of these cells. For example, an increase in the monoclinic angle β for all three twins is not possible short of cleaving the crystal because the lattices would no longer match. Nevertheless, the observation of Bragg peak splitting below $T_{LT}\simeq 175$ K (Ref. 12) implies that a distortion eventually takes place. Its nature likely depends on the shape of in-plane domain boundaries and relative domain population, which has yet to be fully elucidated.

TABLE I. Vibrational modes predicted from a group theoretical analysis according to the symmetry and lattice structure of $LuFe_2O_4$ (Ref. 8). The *z* direction is chosen as $(001)_h$, and *x* is chosen to be the intersection between the mirror plane of the low-temperature $C2/m$ cell and the hexagonal basal plane.

Predicted activity	High temperature $R\bar{3}m$, No. 166	Low temperature $C2/m$, No. 12
Infrared active	$3E_u(x,y)$, $3A_{2u}(z)$	$27A_u(x)$, $36B_u(y,z)$
Raman active	$3A_{1g}(zz)$, $3E_g(xx\text{-}yy,xy)$	$32A_g(xx)$, $28B_g(xy,xz)$

Associated with cell enlargement and symmetry lowering is a splitting of atomic sites (for Wyckoff positions, see Table III, Appendix). For example, in the high-temperature structure, iron has a single position, with $3m$ (threefold rotation and mirror) site symmetry, becoming just *m* after removal of the rotation axis. Tripling *b* splits the Fe site into two different positions, one with and one without mirror symmetry, and doubling *c* further doubles the positions without changing their symmetry. The four sites correspond to Fe^{2+} and Fe^{3+} minorities, with mirror symmetry, and $Fe^{2+/3+}$ majorities at general positions. For the ferroelectric CO, suggested[8] to describe short-range correlations at higher temperature, there are also four sites, with the cell doubling along *c* replaced by removal of the twofold rotation axis.

The vibrational modes predicted by group theoretical analysis are listed in Table I.[29] Assuming every Fe has static charge, the high-temperature phase has 12 modes.[16] This includes three in-plane (E_u) doubly degenerate modes and three out-of-plane (A_{2u}) modes that are infrared active. These results are in agreement with the findings of Harris and Yildirim[16] but different from those of Vitucci *et al.*[10] The displacement patterns of the in-plane (E_u) symmetry infrared-active modes are shown in Fig. 2(a). Because the LuO_2 and Fe_2O_2 (W) layers are connected in a perpendicular fashion, the in-plane LuO_2 and Fe_2O_2 modes are nearly decoupled. The other mode corresponds to relative motion between LuO_2 and Fe_2O_2 layers.[16] The low frequency and modest intensity derive from the small charge/mass ratio. For the low-temperature phase with charge order, the primitive cell is six times larger than that of the high-temperature phase. The $C2/m$ symmetry lifts all degeneracies.[30] Clearly, many modes are expected, different from the results of Vitucci *et al.*[10]

B. Vibrational properties of $LuFe_2O_4$

1. Vibrational spectra and high symmetry mode assignment

Figure 3 displays the measured reflectance and imaginary part of the dielectric function of $LuFe_2O_4$, $\mathcal{R}(\omega)$ and $\varepsilon_2(\omega)$, at three characteristic temperatures.[22] Because our measurements were carried out on the $(001)_h$ crystal face, only in-plane mode contributions are probed. As discussed above,

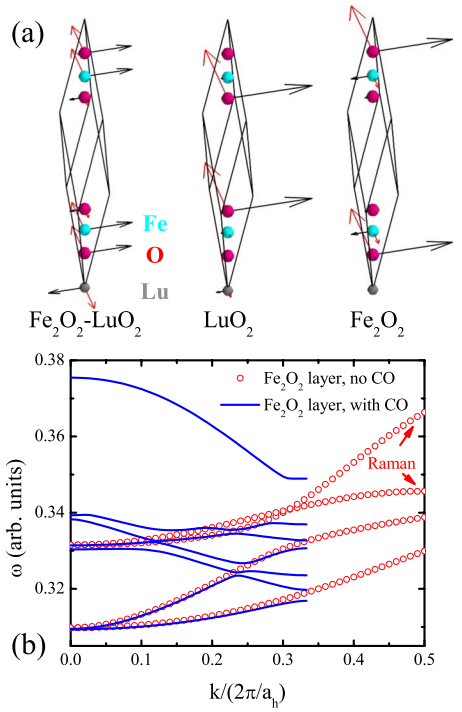

FIG. 2. (Color online) (a) Schematic view of the in-plane (E_u) vibrational modes of $R\bar{3}m$ symmetry. The displacement patterns shown correspond to the Γ (zone-center) point. Here, dark (black) and light (red) arrows correspond to two independent modes with different polarizations. The high-temperature phase primitive cell is superimposed for clarity. (b) Calculated phonon dispersion of isolated Fe_2O_2 with and without charge order along $(100)_h$ direction. The infrared-active modes are shown for the (low-temperature) charge-ordered structure whereas both the infrared- and Raman-active modes are shown for the (high-temperature) charge-disordered case.

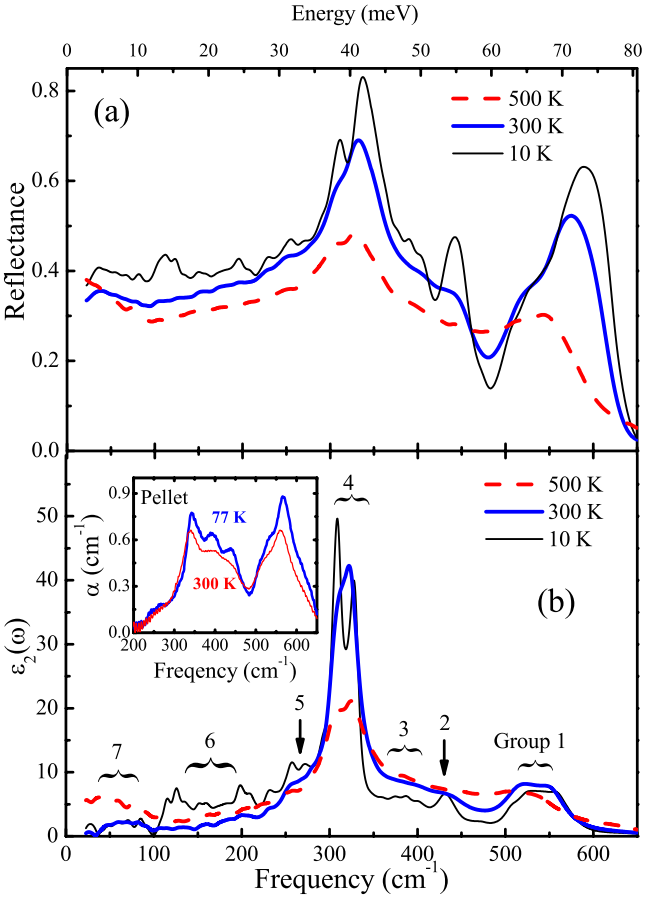

FIG. 3. (Color online) (a) Near-normal reflectance of $LuFe_2O_4$, $\mathcal{R}(\omega)$, measured on the $(001)_h$ crystal face. (b) Imaginary part of the complex dielectric function, $\varepsilon_2(\omega)$, at various temperatures, calculated from the measured reflectance by a Kramers-Kronig analysis. The vibrational features are grouped according to their frequency and temperature dependence. Inset: absorption spectrum of $LuFe_2O_4$ powder embedded in a paraffin matrix.

group theory predicts three well-defined spectral features with E_u symmetry corresponding to (i) relative in-plane shearing motion between the LuO_2 and Fe_2O_2 layers, (ii) in-plane motion within the LuO_2 layer, and (iii) in-plane motion within the Fe_2O_2 layer [Table I, Fig. 2(a)]. At 500 K, the experimental $\varepsilon_2(\omega)$ spectrum does indeed contain three features. These include a weak low-frequency peak at ~70 cm^{-1}, a sharp peak near 320 cm^{-1}, and a broad shoulder at higher frequency. Based upon position and intensity, one can easily assign the weak low-frequency peak as inter-LuO_2/Fe_2O_2 layer motion. Assignment of the anticipated intra-LuO_2 and intra-Fe_2O_2 layer modes is more challenging because the observed line shapes are rather unusual. The problem can be resolved by reconsidering the assumption of static charge. Nominally 2.5+ in the high temperature phase, the Fe site charge has an average rather than static valency due to fluctuations. Because a typical vibrational frequency (10^{12}–10^{13} Hz) (Ref. 31) is much faster than the charge fluctuation in $LuFe_2O_4$(10^6–10^7 Hz),[12] spectral features related to the Fe_2O_2 layers should reflect charge fluctuations. The LuO_2-related feature, by contrast, should be much less sensitive to fluctuations. Thus, one expects a well-defined LuO_2 layer mode and a broad feature emanating from FeO layer motion. We therefore assign the 320 cm^{-1} peak to in-plane motion of the LuO_2 layer. Assignment of intra-Fe_2O_2 motion is less obvious because it is hidden in the broad shoulder at 500 K. Our shell model calculations provide numerical support for these assignments. Lu-Fe, LuO_2, and Fe_2O_2 blocks are predicted at 68, 320, and 520 cm^{-1} in reasonable agreement with the values obtained by Harris and Yildirim[16] (92, 332, and 474 cm^{-1}). This relative ordering of the intra-LuO_2 vs intra-Fe_2O_2 layer modes is in line with mass arguments.

In order to precisely locate the intra-Fe_2O_2 modes, one has to examine the low-temperature phase response and consider the relation between the mode distribution and the primitive cell. Low-temperature charge order expands (shrinks) the primitive cell (Brillouin zone) by a factor of 6 compared to the high-temperature phase. The folded modes thus display a finite polarization due to charge-order-induced symmetry breaking. The latter also activates some Raman features that emanate from the high-temperature symmetric phase. Figure 2(b) displays the calculated phonon dispersion of an isolated Fe_2O_2 layer.[32] Both infrared- and Raman-

TABLE II. Summary of spectral features observed in $\varepsilon_2(\omega)$ for $LuFe_2O_4$.

Group	7	6	5	4	3	2	1
Frequency (cm^{-1})	broad ~70	144–257	270, 292	308, 326	360, 374, 388, 400	430	530, 560
Assignment	LuO_2-Fe_2O_2 layer shear			LuO_2 in-plane	LuO_2 zone folding	Fe_2O_2 in-plane	Fe_2O_2 zone folding

active modes are plotted for the noncharge ordered structure. In the charge-ordered phase, we plot only the infrared-active modes. Due to the upward curvature of the Fe_2O_2 layer phonon dispersion, infrared-active zone-folded modes (thin solid lines in Fig. 2) appear at higher frequencies than the fundamentals. This observation suggests that groups 1, 2, and 3 (Fig. 3) should be assigned as Fe_2O_2 zone-folding modes, Fe_2O_2 in-plane modes, and LuO_2 zone-folding modes, respectively. The directional characteristics are in line with these assignments.[33] Table II summarizes our results.

2. LuO_2 *in-plane fundamental modes and antipolar bilayer stacking in* $LuFe_2O_4$

Figure 4(a) displays a closeup view of the group 4 doublet in $\varepsilon_2(\omega)$. These features are assigned as LuO_2 layer modes. At 500 K, both components of the doublet are broad and low due to fluctuations. Their temperature dependence is, however, quite different [Fig. 4(b)]. The intensity of 308 cm^{-1} component is small above T_{CO}, increases with decreasing temperature below T_{CO}, reaches a maximum at T_{LT}, and saturates at low temperature. In contrast, the intensity of the 326 cm^{-1} component reaches a maximum at T_{CO} and drops with decreasing temperature before saturating at low temperature.[23]

Three different scenarios immediately arise that can account for the observed doublet structure. They include: (i) in-plane anisotropy effects on the LuO_2 layer modes due to ferroelectric charge order (essentially the difference between parallel and perpendicular polarizations with respect to the mirror plane), (ii) long-range intralayer charge disproportionation in which both layers of a bilayer are 2+ rich and both layers of the next bilayer are 3+ rich, and (iii) the presence of two distinct LuO_2 layer environments corresponding to an antipolar arrangement of W layers. Lattice dynamics calculations reveal that the effect from mechanism (i) is too small to generate the observed 18 cm^{-1} splitting. Moreover, relative changes in doublet intensities with temperature would be expected to be similar, an expectation that is clearly inconsistent with observation [Fig. 4(b)]. On the other hand, mechanism (ii) could generate a sizable splitting, but it would imply interdouble-layer charge transfer, a scenario therefore excluded in previous structural analysis.[8] Mechanism (iii) also supports sizable mode splitting. Dynamics calculations provide a way forward with respect to the temperature-dependent peak intensities by suggesting that the two independent LuO_2 layers in the antipolar cell generate two kinds of modes by superposition. In the high-temperature phase, the Fe_2O_2 layers do not have electric dipoles, so the two LuO_2 layers are equivalent. Therefore, the superposition generates one Raman-active and one infrared-active mode as depicted in Fig. 4(c). When temperature is decreased, symmetry is reduced due to charge ordering, and the Raman mode becomes infrared active. Thus, a new peak emerges below T_{CO} that steals oscillator strength from the original infrared-active band. At low temperature, the two LuO_2 layers are inequivalent. One type of LuO_2 layer is sandwiched between charge-rich FeO slabs, whereas the other type is sandwiched between charge-poor FeO layers. When charge order is strong enough, the two types of modes correspond to intra-LuO_2 motion of the two distinct LuO_2 layers, as depicted in Fig. 4(d). As we discuss below, this scenario clearly excludes standard ferroelectric stacking of the W layers. The intensities of LuO_2 layer modes in prox-

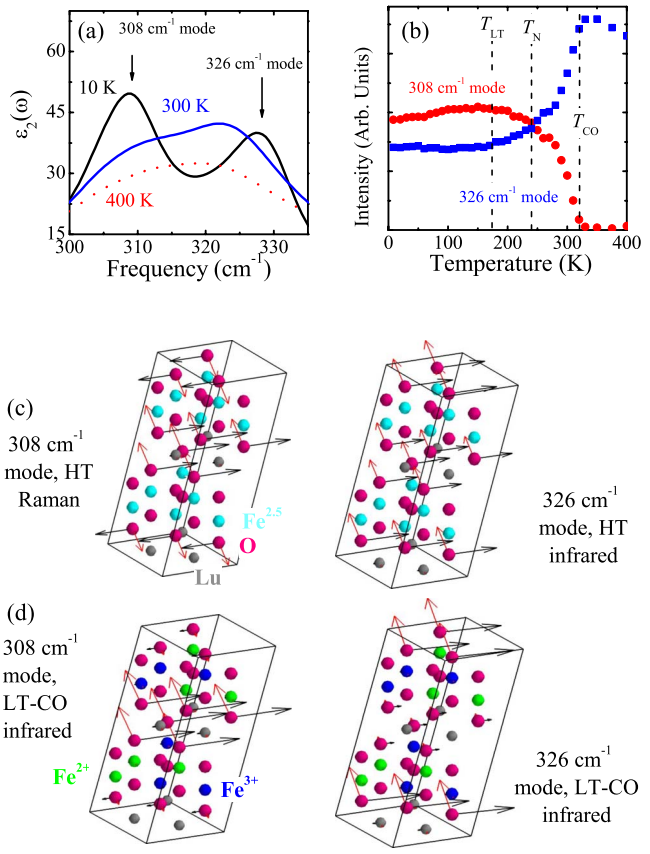

FIG. 4. (Color online) (a) Closeup view of $\varepsilon_2(\omega)$ showing the in-plane LuO_2 modes. (b) Temperature dependence of peak intensity. These data were determined from oscillator fits (Ref. 23). Relative error bars are on the order of the symbol size. (c) and (d) show calculated displacement patterns for the (high-temperature) charge-disordered phase and (low-temperature) charge-ordered phase, respectively. In (c), the left- (right-) hand pattern corresponds to a Raman (infrared) active mode. In (d), both are infrared active due to symmetry breaking. Here, dark (black) and light (red) arrows indicate two independent modes with different polarizations.

imity to charge-rich/poor iron oxide layers should be similar at low temperature.

Comparing the temperature dependence of the 308 and 326 cm^{-1} components with the above predictions, we can assign the microscopic nature of each peak. The intensity of the 308 cm^{-1} component increases with decreasing temperature below T_{CO}, in line with predictions for a feature originating from a high symmetry Raman-active mode, mainly from LuO_2 sandwiched between charge-poor FeO layers at low temperature. The 326 cm^{-1} component, on the other hand, behaves in the opposite way, perfectly consistent with the other mode, deriving mainly from LuO_2 sandwiched between charge-rich FeO layers at low temperature. The proximity effect observed here, with the charge-rich (poor) layer resonating at higher (lower) frequency, is consistent with observations in other model materials.[34] The strong coupling between the charge order and the LuO_2 vibrational modes makes the latter a unique probe of charge order.

Importantly, the doublet character of the LuO_2 layer mode, its temperature dependence, and our assignment in terms of proximity to charge-rich and charge-poor FeO layers is in line with expectations for an antipolar ground state in $LuFe_2O_4$.[8] It is inconsistent with ferroelectric ordering of the W layers.[35] The mode behavior also rules out any other similar kind of interlayer charge ordering. For instance, the ferrielectric arrangement proposed by Xiang *et al.*[11] would produce three unique components to the LuO_2 intralayer vibrational pattern rather than the two found in experiment. In addition, the LuO_2 features are in-plane polarized, as shown by a comparison between single crystal and powder sample spectra (inset, Fig. 3).[33] Taken together, these findings suggest that antipolar ordering of the Fe_2O_2 bilayers is the most likely arrangement, consistent with the observed temperature-dependent vibrational spectra.[36]

3. LuO_2 zone-folding modes couple strongly to the charge order, magnetism, and structural distortion

Figure 5(a) displays a closeup view of $\varepsilon_2(\omega)$ in the regime corresponding to LuO_2 zone-folding modes of $LuFe_2O_4$ (group 3). The spectrum is relatively flat at high temperature due to disorder and the high symmetry created by fluctuation. At least three peaks emerge at low temperature. The calculated peak area is shown in Fig. 5(b).[37] Besides a cusp at 320 K and a minimum just above T_{CO}, the peak area is very sensitive to magnetic order at T_N and the structural distortion at T_{LT}.

Figure 5 also shows the displacement patterns of two example LuO_2 zone-folding modes suggested from calculation. Panel (c) shows a LuO_2 layer twisting mode and panel (d) shows a combined LuO_2+Fe_2O_2 layer twisting mode. In the high-temperature (high symmetry) phase, these modes are infrared inactive. The reduced symmetry of the low-temperature charge-ordered phase gives rise to mode polarization. Zone-folding modes are thus anticipated to be very sensitive to structural symmetry.

These predictions are consistent with our experimental observations. Above T_{CO}, high symmetry and strong fluctuation obscures individual components of the LuO_2 zone-folding modes. Below T_{CO}, charge-order-induced symmetry lowering results in distinct peaks. Interestingly, when temperature is reduced below T_N, the peak area vs temperature trend is reversed. This is because charge order is damped by the development of magnetic order. The competition between charge and magnetic order is also seen in x-ray diffraction experiments and terahertz time-domain spectroscopy.[8,9] Further, like the 1 THz soft mode observed by Li *et al.*,[9] LuO_2 zone-folding modes are of correct symmetry to contribute to the small polarization and dielectric changes at 240 and 175 K.[2,5] Below T_{LT}, peak area increases on cooling, consistent with enhanced charge order and structural distortion.[8,9,12]

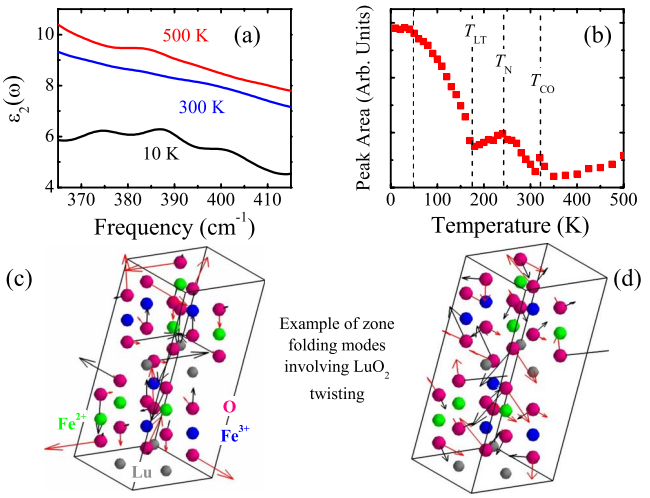

FIG. 5. (Color online) (a) Closeup view of $\varepsilon_2(\omega)$ showing features that we assign as LuO_2 zone-folding modes. (b) Temperature dependence of the peak area. These data were determined from oscillator fits (Ref. 23). Relative error bars are on the order of the symbol size. (c) and (d) show typical calculated displacement patterns of LuO_2 zone-center modes in the (low-temperature) charge-ordered phase.

4. Probing intralayer charge order: The Fe_2O_2 fundamental and zone-folding modes

Figure 6(a) displays a closeup view of $\varepsilon_2(\omega)$ in the group 2 spectral regime. This structure is assigned as Fe_2O_2 in-plane motion. We find that the area of this feature is sensitive to charge ordering at 320 K [Fig. 6(b)] but only weakly coupled to T_N and T_{LT}. This is because charge-order-induced symmetry breaking transfers a small portion of the Fe_2O_2 in-plane mode oscillator strength to the zone-folding modes, an effect that gives extra sensitivity to symmetry modifications. Figure 6(e) shows the calculated displacement pattern of the Fe_2O_2 layer mode in the low-temperature charge-ordered phase. Our calculations predict a significant out-of-plane component to the displacement, indicative of lower symmetry. The Born effective charge calculated from the observed mode intensity[38] is $q_{eff}=1.5e^-$ at 10 K, less than the nominal Fe center valence in this material. This result implies that $LuFe_2O_4$ is less ionic than simple valence counting schemes might predict, different than the conclusion of Mulders *et al.*[14] where a 4 eV chemical shift of the Fe *K* edge indicates fully ionic valence states.

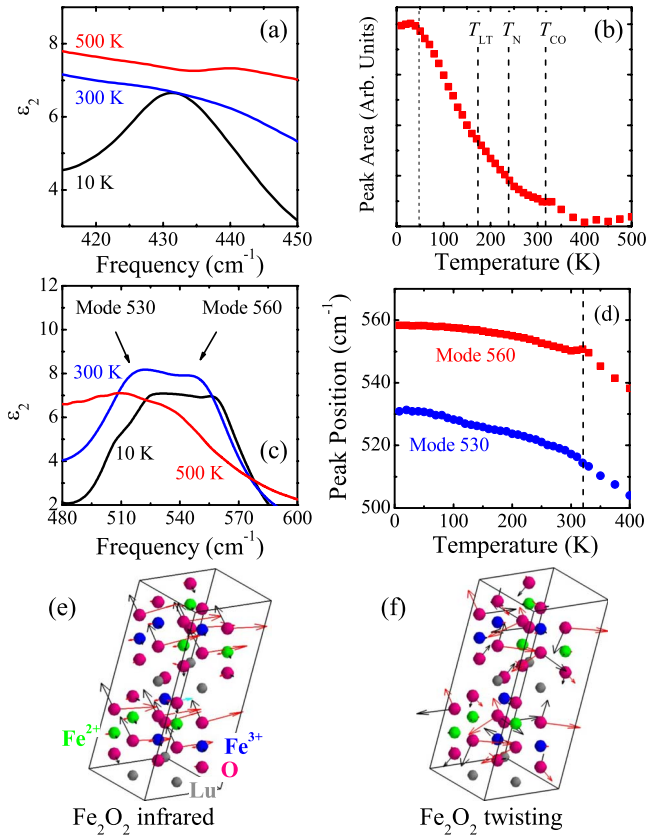

FIG. 6. (Color online) (a) Closeup view of $\varepsilon_2(\omega)$ showing the Fe_2O_2 in-plane modes. (b) Peak area vs temperature for the Fe_2O_2 in-plane modes. These data were determined from oscillator fits (Ref. 23). Relative error bars are on the order of the symbol size. (c) Closeup view of $\varepsilon_2(\omega)$ showing the Fe_2O_2 zone-folding modes. (d) Frequency vs temperature of two Fe_2O_2 zone-folding modes. As before, these data were determined from oscillator fits (Ref. 23). (e) Calculated displacement patterns of Fe_2O_2 in-plane modes in the (low-temperature) charge-ordered phase. (f) Example displacement patterns for Fe_2O_2 zone-folding modes in the (low-temperature) charge-ordered phase.

Figure 6(c) displays a closeup view of the Fe_2O_2 zone-folded modes of $LuFe_2O_4$ (group 1). As anticipated from our dispersion calculations, this structure is a superposition of more than one oscillator. The Fe_2O_2 twisting pattern shown in Fig. 6(f) is an example of the type of motion involved. The behavior of these Fe_2O_2 zone-folding modes is unique in that there is a significant temperature-induced frequency shift. We quantified this effect by fitting the spectral features with two oscillators up to 400 K. The results are shown in Fig. 6(d). Both components redshift strongly on warming, a trend that is not as obvious in other modes. At T_{CO}, the mode frequencies drop more quickly, an indication of mode instability and a sign of a structural or bonding transition driven by elevated temperature.[39] Intensity changes are observed as well [Fig. 6(c)]. A similar group of modes is observed in the spectra of Vitucci *et al.* The splitting is more pronounced but they do not offer a mode assignment.[10] We attribute this difference to sample quality issues.[40] Recently, Harris and Yildirim[16] predicted that a low-frequency Raman-active mode of E_g symmetry (in the rhombohedral unit cell, Table I) should couple most effectively to the charge ordering. Due to charge fluctuations, however, one actually has to consider more than the modes in rhombohedral cell because the low symmetry modes already exist even at high temperature. For example, the features shown in Fig. 6(c) may also couple strongly to the 3D charge ordering.

5. Frozen lattice response below 50 K

As discussed above, the lattice vibrations of $LuFe_2O_4$ are very sensitive to the series of temperature-driven transitions: 320 K (T_{CO}), 240 K (T_N), and 175 K (T_{LT}). In addition, the entire spectrum freezes at $T \sim 50$ K. The lack of change in the dynamical response is shown most clearly in the Fe_2O_2 fundamental and the LuO_2 zone-folding modes [Figs. 6(b) and 5(b), respectively]. This indicates that the structural distortion, charge order, and the fluctuation of the charge order remain constant below 50 K, a finding that may be related to the emergence of a glassy state, a state with unusual domain structure, or perhaps an interesting antiferromagnetic state.[2,9,41–43] In the former two scenarios, the freezing of the spectrum is likely tied to the kinetic arrest of the magneto-structural transition discussed in Ref. 12. By way of comparison, the perovskite $CaCu_3Ti_4O_{12}$ displays relaxorlike dynamical slowing down of the dipolar fluctuations on approach to a frozen, glasslike state.[44] Clearly, more investigation is needed to understand the nature of this regime in $LuFe_2O_4$.

IV. SUMMARY

We investigated the vibrational response of $LuFe_2O_4$ through the series of temperature driven transitions using infrared spectroscopy and compared our results with complementary group theoretical predictions and lattice dynamics calculations. The LuO_2 layer mode is particularly sensitive to charge proximity effects with temperature-driven changes in the oscillator strength of the doublet structure that reveal antipolar ordering of the Fe_2O_2 bilayers rather than the previously supposed ferroelectric alignment. Analysis of LuO_2 zone-folding and Fe_2O_2 layer mode trends indicate that charge order couples strongly to and competes with magnetism. We discuss our findings in comparison to other model materials.

ACKNOWLEDGMENTS

This work was supported by the Division of Materials Science and Engineering, Basic Energy Sciences, U.S. Department of Energy (UT and ORNL), the State of Texas through the Texas Center for Superconductivity (UH), and the Initiative and Networking Fund of the Helmholtz Association of German Research Centers through the Helmholtz-University Young Investigator Group Complex Ordering Phenomena in Multifunctional Oxides (Jülich).

APPENDIX: WYCKOFF SITES

For Wyckoff positions, see Table III.

TABLE III. Splitting of Wyckoff positions due to charge order. For domain A with propagation vector $(\frac{1}{3}\frac{1}{3}\frac{3}{2})_h$, the lattice parameters transform as $\mathbf{a}_A=\mathbf{a}_h-\mathbf{b}_h$, $\mathbf{b}_A=3(\mathbf{a}_h+\mathbf{b}_h)$, and $\mathbf{c}_A=\frac{2}{3}(-\mathbf{a}_h+\mathbf{b}_h+\mathbf{c}_h)$. For the atom sites shown, we give Wyckoff labels (site symmetry) and coordinates of a representative in fractions of the respective cell. Greek symbols and decimal point numbers are freely adjustable parameters.

Site	Wyckoff	Representative
	High-T structure ($R\bar{3}m$)	
Lu	$3a$ $(-3m)$	(0,0,0)
Fe	$6c$ $(3m)$	$(0,0,\zeta)$
O1	$6c$ $(3m)$	$(0,0,\zeta)$
O2	$6c$ $(3m)$	$(0,0,\zeta)$
	CO structure, domain A ($C2/m$)	
Lu	$2a$ $(2/m)$	(0,0,0)
	$4g$ (2)	(0,0.333,0)
	$2c$ $(2/m)$	$(0,0,\frac{1}{2})$
	$4h$ (2)	$(0,0.333,\frac{1}{2})$
Fe	$4i_1$ (m)	$(\zeta,0,\frac{3}{2}\zeta+\eta)$
	$8j_1$ (1)	$(\zeta,0.333,\frac{3}{2}\zeta+\eta)$
	$4i_2$ (m)	$(\zeta,0,\frac{3}{2}\zeta+\eta+\frac{1}{2})$
	$8j_2$ (1)	$(\zeta,0.333,\frac{3}{2}\zeta+\eta+\frac{1}{2})$
O1	$4i_1$ (m)	$(\zeta,0,\frac{3}{2}\zeta+\eta)$
	$8j_1$ (1)	$(\zeta,0.333,\frac{3}{2}\zeta+\eta)$
	$4i_2$ (m)	$(\zeta,0,\frac{3}{2}\zeta+\eta+\frac{1}{2})$
	$8j_2$ (1)	$(\zeta,0.333,\frac{3}{2}\zeta+\eta+\frac{1}{2})$
O2	$4i_1$ (m)	$(\zeta,0,\frac{3}{2}\zeta+\eta)$
	$8j_1$ (1)	$(\zeta,0.333,\frac{3}{2}\zeta+\eta)$
	$4i_2$ (m)	$(\zeta,0,\frac{3}{2}\zeta+\eta+\frac{1}{2})$
	$8j_2$ (1)	$(\zeta,0.333,\frac{3}{2}\zeta+\eta+\frac{1}{2})$

*Present address: Oak Ridge National Laboratory, Oak Ridge, TN.

[1] J. van den Brink and D. I. Khomskii, J. Phys.: Condens. Matter **20**, 434217 (2008).
[2] J. Iida, M. Tanaka, Y. Nakagawa, S. Funahashi, N. Kimizuka, and S. Takekawa, J. Phys. Soc. Jpn. **62**, 1723 (1993).
[3] N. Ikeda, H. Ohsumi, K. Ohwada, K. Ishii, T. Inami, K. Kakurai, Y. Murakami, K. Yoshii, S. Mori, Y. Horibe, and H. Kito, Nature (London) **436**, 1136 (2005).
[4] M. A. Subramanian, T. He, J. Z. Chen, N. S. Rogado, T. G. Calvarese, and A. W. Sleight, Adv. Mater. **18**, 1737 (2006).
[5] C.-H. Li, X.-Q. Zhang, Z.-H. Cheng, and Y. Sun, Appl. Phys. Lett. **92**, 182903 (2008).
[6] K.-T. Ko, H.-J. Noh, J.-Y. Kim, B.-G. Park, J.-H. Park, A. Tanaka, S. B. Kim, C. L. Zhang, and S.-W. Cheong, Phys. Rev. Lett. **103**, 207202 (2009).
[7] A. D. Christianson, M. D. Lumsden, M. Angst, Z. Yamani, W. Tian, R. Jin, E. A. Payzant, S. E. Nagler, B. C. Sales, and D. Mandrus, Phys. Rev. Lett. **100**, 107601 (2008).
[8] M. Angst, R. P. Hermann, A. D. Christianson, M. D. Lumsden, C. Lee, M.-H. Whangbo, J.-W. Kim, P. J. Ryan, S. E. Nagler, W. Tian, R. Jin, B. C. Sales, and D. Mandrus, Phys. Rev. Lett. **101**, 227601 (2008).
[9] S. Z. Li, S. J. Luo, R. Fu, B. B. Jin, K. F. Wang, J.-M. Liu, J. F. Ding, and X. G. Li, Appl. Phys. A **96**, 893 (2009).
[10] F. M. Vitucci, A. Nucara, D. Nicoletti, Y. Sun, C. H. Li, J. C. Soret, U. Schade, and P. Calvani, Phys. Rev. B **81**, 195121 (2010).
[11] H. J. Xiang and M.-H. Whangbo, Phys. Rev. Lett. **98**, 246403 (2007).
[12] X. S. Xu, M. Angst, T. V. Brinzari, R. P. Hermann, J. L. Musfeldt, A. D. Christianson, D. Mandrus, B. C. Sales, S. McGill, J.-W. Kim, and Z. Islam, Phys. Rev. Lett. **101**, 227602 (2008).
[13] H. Yang, Y. Zhang, Y. Qin, C. Ma, H. Tian, and J. Li, Phys. Status Solidi B **247**, 870 (2010).
[14] A. M. Mulders, S. M. Lawrence, U. Staub, M. Garcia-Fernandez, V. Scagnoli, C. Mazzoli, E. Pomjakushina, K. Conder, and Y. Wang, Phys. Rev. Lett. **103**, 077602 (2009).
[15] A. Nagano, M. Naka, J. Nasu, and S. Ishihara, Phys. Rev. Lett. **99**, 217202 (2007).
[16] A. B. Harris and T. Yildirim, Phys. Rev. B **81**, 134417 (2010).
[17] E. Ya. Sherman, M. Fischer, P. Lemmens, P. H. M. van Loosdrecht, and G. Güntherodt, Europhys. Lett. **48**, 648 (1999).
[18] C. Presura, D. van der Marel, A. Damascelli, and R. K. Kremer, Phys. Rev. B **61**, 15762 (2000).
[19] We describe the magnetic arrangement as "antipolar" rather than "antiferroelectric" (which is sometimes used in the literature and may be more widely known) in order to clearly indicate the lack of electric field switchability in $LuFe_2O_4$.

[20] Our measurements were carried out at a 6° angle of incidence with respect to an aluminum mirror. The resulting reflectance was corrected for the finite reflectance of aluminum.
[21] F. Wooten, *Optical Properties of Solids* (Academic Press, New York, 1972).
[22] This function is related to optical conductivity as $\epsilon(\omega)=\epsilon_1(\omega)+i\epsilon_2(\omega)=\epsilon_1(\omega)+\frac{4\pi i}{\omega}\sigma_1(\omega)$.
[23] See supplementary material at http://link.aps.org/supplemental/10.1103/PhysRevB.82.014304 for several example fits as shown in the electronic auxiliary material.
[24] D. Wolf, P. Keblinski, S. R. Philpot, and J. Eggebrecht, J. Chem. Phys. **110**, 8254 (1999).
[25] J. D. Gale and A. L. Rohl, Mol. Simul. **29**, 291 (2003).
[26] J. Cao, L. I. Vergara, J. L. Musfeldt, A. P. Litvinchuk, Y. J. Wang, S. Park, and S. W. Cheong, Phys. Rev. B **78**, 064307 (2008).
[27] We use the commensurate approximation as in Ref. 8.
[28] Optimization of corresponding refinement of atom positions is still ongoing and complete results will be given elsewhere.
[29] W. G. Fateley, *Infrared and Raman Selection Rules for Molecular and Lattice Vibrations: The Correlation Method* (Wiley-Interscience, New York, 1972).
[30] The unique direction is along x in the low-temperature phase rather than along z as in the high temperature. Here, x axis is the line intersecting the basal plane and the mirror plane, and z is the $(001)_h$ direction.
[31] V. C. Long, J. L. Musfeldt, K. Kamarás, A. Schilder, and W. Schütz, Phys. Rev. B **58**, 14338 (1998).
[32] J. D. Bailey and J. Patteson, *Solid-State Physics: Introduction to the Theory* (Springer, Berlin, 2006).
[33] As shown in the inset of Fig. 3, the absorption spectra of powder sample show enhanced intensity of group 1 and 3 compared with group 2 and 4, indicating that the polarization of group 1 and 3 are more out of plane, consistent with the assignment of zone-folding modes, which come from the low symmetry of the charge order.
[34] J. L. Musfeldt, K. Kamarás, and D. B. Tanner, Phys. Rev. B **45**, 10197 (1992).
[35] In this case, group theory predicts only one component to the intralayer LuO_2 mode, a result that is clearly incompatible with our experimental observation.
[36] All the following discussion will be in the context of antipolar CO.
[37] The peak area is calculated by fitting the peak in a certain range with a straight baseline. In this way, the background contribution can be excluded, only the sharpness of the peak is retained.
[38] X. S. Xu, Q. C. Sun, R. Rosentsveig, and J. L. Musfeldt, Phys. Rev. B **80**, 014303 (2009).
[39] J. F. Scott, Rev. Mod. Phys. **46**, 83 (1974).
[40] Our crystals were grown in CO/CO_2 flow rather than Ar, a procedure that gives us excellent control over oxygen stoichiometry. Considering the different synthetic procedures, it is very likely that our samples and Vitucci *et al.*'s are not equivalent. Moreover, our crystals display typical quality indicators such as magnetic ordering at $T_N=240$ K (rather than 230 K) and a clear T_{LT} transition that can be deduced even in the infrared spectra. The low-frequency reflectance is also relatively flat, another indication of nonleaky samples.
[41] M. H. Phan, N. A. Frey, M. Angst, J. de Groot, B. C. Sales, D. G. Mandrus, and H. Srikanth, Solid State Commun. **150**, 341 (2010).
[42] S. Park, Y. Horibe, Y. J. Choi, C. L. Zhang, S.-W. Cheong, and W. Wu, Phys. Rev. B **79**, 180401(R) (2009).
[43] Y. Matsuo, S. Shinohara, S. Mori, Y. Horibe, K. Yoshii, and N. Ikeda, in *Ferroelectrics and Multiferroics*, edited by V. Gopalan, J.-P. Maria, M. Fiebig, and C.-W. Nan, MRS Symposia Proceedings No. 966E (Materials Research Society, Warrendale, 2007).
[44] C. C. Homes, T. Vogt, S. M. Shapiro, S. Wakimoto, and A. P. Ramirez, Science **293**, 673 (2001).